Photothermal properties of Fe_3O_4 nanoparticles coated with turmeric extract

M. L. Alvarado-Noguez*, A. E. Matías-Reyes, A. Cruz-Orea, and J. Santoyo-Salazar
Departamento de Física, Centro de Investigación y de Estudios Avanzados-IPN,
Av. IPN No. 2508, Col. San Pedro Zacatenco, 07360 Ciudad de México, México.
**e-mail: margarita.alvarado@cinvestav.mx*

F. A. Domínguez-Pacheco and C. Hernández-Aguilar
Instituto Politécnico Nacional - SEPI-ESIME, Zacatenco,
Edificio 5, 3er Piso, Unidad Profesional "Adolfo López Mateos". Col. Lindavista,
Ciudad de México 07738, México., México.

A. A. Duran-Ledezma
Instituto Politécnico Nacional - SEPI-ESIME, Ticomán,
Av. Ticomán No. 600, San José Ticomán, 07340, Gustavo A. Madero, Ciudad de México, México.

Received 28 April 2023; accepted 1 August 2023

In this study, we synthesized magnetite nanoparticles through a modified coprecipitation route and subsequently coated them directly with *Curcuma longa* extract. The resulting nanoparticles were then dispersed in distilled water to create a nanofluid. The particle size distribution ranged between 9 to 18 nm according to Transmission Electron Microscopy and Dynamic Light Scattering. The nanofluid's thermal parameters were obtained by photothermal techniques, obtaining their thermal diffusivity, effusivity, conductivity, and heat capacity per unit volume. The Thermal Wave Resonator Cavity was employed to measure the thermal diffusivity, while the Inverse Photopyroelectric photothermal technique was used to determine the effusivity value. The obtained thermal parameters were close to the carrier liquid (distilled water), being a preliminary study that can be analyzed to improve the heat transfer application in other suspension fluids.

Keywords: Magnetite; nanoparticles; curcuma longa; photopyroelectric technique; thermal diffusivity; thermal effusivity.

DOI: https://doi.org/10.31349/RevMexFis.70.011601

1. Introduction

Superparamagnetic iron oxide nanoparticles (SPIONs) are widely used in the development of medical formulations and have been regulated by the US Food and Drug Administration (FDA) for medical purposes [1]. Magnetite nanoparticles (MNPs) are primarily used in drug delivery and hyperthermia therapy because of their solid magnetic responsiveness, good biocompatibility, and low toxicity [2]. Also, MNPs have been studied in the engine industry, observing the enhanced physicochemical and phytochemical properties in biofuel addition; and engine performance [3]. Several magnetite formulations have been developed to improve colloidal stability and physicochemical properties [4–7]. The eco-friendly synthesis of MNPs from plant extracts stands out for their less toxic synthesis waste and low cell toxicity [8, 9]. Green synthesis of magnetic nanoparticles also helps in the energy-sustainable sector through their application in bio-additives, biofuels, Enzymatic biocatalysis, etc. [10–12]. Flavonoids are natural polyphenolic compounds very effective in preventing and controlling cancer diseases, and it has been reported that phytochemical elements add organic chains, which helps in the reduction reaction during the magnetite synthesis process [9, 13, 14]. Turmeric (*Curcuma longa L.*) belongs to the Zingiberaceae family and mainly comprises the following natural polyphenols: curcumin, demethoxycurcumin, and bisdemethoxycurcumin [15]. Curcumin ($C_{21}H_{20}O_6$) is the main component of Turmeric, extensively explored for its therapeutic potential, such as antioxidant, anti-inflammatory, antimicrobial, and anticancer properties, as well as thermal insulation properties [6, 16–18]. Also, turmeric has been used for biodiesel and biofuel production and as a fuel additive, improving engine efficiency, retarding the oxidation process, and reducing costs and emissions [3, 19, 20]. Recently, there has been an increased focus on the thermophysical properties of MNPs due to their application as targeted thermal agents in alternative therapies, photothermal-activated drug delivery, and the biofuel industry [20–23]. The key thermal parameters include thermal conductivity, diffusivity, and effusivity, which are essential for quantitative analysis and extracting information about the material microstructure of the nanoparticles [21, 22]. The photopyroelectric (PPE) setup is a high-sensitivity, adaptable, and non-destructive technique, that has been widely acknowledged as a powerful tool for high-resolution measurements of material thermal properties. In this study, semi-spherical magnetite nanoparticles were coated with Curcuma longa extract ($C_{96}H_{104}O_{20}$) via a coprecipitation-modified route. $C_{96}H_{104}O_{20}$ was linked to MNPs by -OH bonds at the metallic ions (Fe-OH). Thermal characterization of this nanofluid will allow us to determine possible applications in heat transport, obtaining their thermal diffusivity and effusivity by Thermal Wave Resonator Cavity (TWRC) and inverse photopyroelectric (IPPE) photothermal techniques, respectively. Thermal conductivity and heat capacity per unit volume were obtained from the thermal diffusivity and effusivity relationships. In addition, complementary characterization to get the shape, organic coating thickness, and size of MNPs coated with Curcuma longa (MNPs@ $C_{96}H_{104}O_{20}$) was obtained by Transmission Electron Microscopy (TEM) and Dynamic Light Scattering (DLS).

2. Materials and methods

2.1. Materials

Ferric trichloride hexahydrate ($FeCl_3\cdot 6H_2O$) (purity, p.a., ≥97%), ferric dichloride tetrahydrate ($FeCl_2\cdot 4H_2O$) (purity, p.a., ≥99%), ethanol, and potassium hydroxide (KOH) were acquired from Sigma-Aldrich. This study used commercial turmeric powder from India (TRS; Curcuma longa powder) and deionized water. All reagents were used as received without any additional purification steps.

2.2. Methods

Turmeric extract preparation

To prepare the turmeric extract, 20 g of Commercial turmeric powder was mixed in 400 mL of ethanol 80%. The mixture was heated to 200°C and stirred magnetically at 400 rpm for 20 min. After the stirring process, the mixture was allowed to cool [21].

Synthesis of MNPs@ $C_{96}H_{104}O_{20}$

$FeCl_3\cdot 4H_2O$ and $FeCl_3\cdot 6H_2O$ were separately mixed in degassed water. After 30 minutes, they were combined in a 3-necked flask maintained at a temperature of 70°C. Subsequently, KOH with a molarity of 7 was added dropwise, followed by adding 50 mL of the previously prepared turmeric extract (TE). The solution was mechanically stirred at 200 rpm to maintain an inert atmosphere and prevent oxidation [8]. Please refer to our recent report [9] for a detailed synthesis method. The resulting solution, which had a black color and a pH of 14, was separated using an external magnetic field (neodymium magnet). It was then subjected to multiple washes with water and ethanol to remove both inorganic and organic impurities. Finally, the solution was lyophilized, resulting in the MNPs@ $C_{96}H_{104}O_{20}$ powder. This powder was subsequently characterized and stored under vacuum conditions.

Synthesis of MNPs

To compare the properties of our system, bare Fe_3O_4 nanoparticles were synthesized using the coprecipitation iron salt method, as described in a separate report [9].

2.3. Particle size and coating

Transmission electron microscopy

The synthesized nanoparticles were subjected to sonication for 10 min. in a distilled water suspension. Subsequently, they were deposited onto a copper grid lacey 400 mesh. The samples were analyzed using a JEOL JEM2010 microscope equipped with a LaB_6 filament operating at 200 keV. The average size of the nanoparticles was determined by measuring 150 particles. The obtained particle size distributions were fitted using a Gaussian function.

Dynamic light scattering

The particles were dispersed in 0.06% citric acid solution. After filtration through a 45 nm nominal pore size (Millipore) to remove suspended impurities and sonication for 15 min at 30°C, the sample solution was placed in a glass cell. The DLS experiments were performed at 20°C constant temperature, at an angle of 130°, using a commercial goniometer-based 3D light scattering instrument (LS instruments AG, Fribourg, Switzerland). The device was equipped with a He-Ne laser as a light source, at a 632.8 nm wavelength, with vertical polarisation.

2.4. Photothermal characterization

Thermal wave resonator cavity for thermal diffusivity (α) measurements

TWRC technique was employed to measure the thermal diffusivity α of the sample [23]. Thermal diffusivity represents the ratio of thermal conductivity to heat capacity per unit volume of the material. The one-dimensional heat diffusion equation derives the theoretical expression for thermal diffusivity.

$$\frac{\partial^2 T}{\partial^2 x} + \frac{1}{\alpha}\frac{\partial T}{\partial x} = 0; \qquad x < 0, \quad t > 0. \tag{1}$$

Additionally, a periodic energy boundary condition is applied to the surface of the sample. This boundary condition ensures that the energy exchange within the sample follows a periodic pattern.

$$-k\frac{\partial T}{\partial x} = \frac{Q_0}{2}[1+\cos(\omega t)] = Re\left\{\frac{Q_0}{2}\left[1+\exp(i\omega t)\right]\right\}; \qquad x=0, \quad t > 0. \tag{2}$$

In Eq. (2) T represents the sample temperature, and κ represents the thermal conductivity. Q_0 denotes the incident light intensity, and $\omega = 2\pi\nu$, where ν represents the modulation frequency of the light. By solving Eq. (1) with the boundary condition expressed in Eq. (2), the solution can be written as:

$$T(x,t) = \frac{Q_0}{2\kappa\sigma}\exp\left(-\sigma x + i\omega t\right), \tag{3}$$

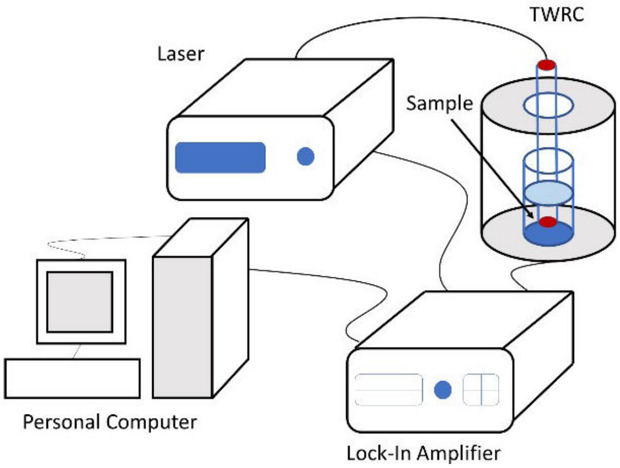

FIGURE 1. Experimental set up of TWRC.

where $\sigma_j = (1+j)a_j$, σ_j: complex thermal diffusion coefficient of material i. $a_j = \sqrt{\pi\nu/\alpha}$, a_j: thermal diffusion coefficient of material.

In polar coordinates, the solution can be expressed as [22]:

$$T(x,t) = \frac{Q_0}{2\sqrt{\rho c\kappa\omega}} \exp\left(-x\sqrt{\frac{\omega}{2\alpha}}\right) \times \exp i\left(\omega t - x\sqrt{\frac{\omega}{2\alpha}} - \frac{\pi}{4}\right). \quad (4)$$

In TWRC experiment (Fig. 1), the photopyroelectric signal is measured as a function of the sample thickness placed inside the TWRC. The amplitude of Eq. (4) is directly associated with the experimental amplitude of the pyroelectric sensor [23].

Inverse photopyroelectric configuration for thermal effusivity (e) measurements

The thermal effusivity e can be measured using the inverse photopyroelectric configuration, utilizing polyvinylidene difluoride (PVDF) as the pyroelectric sensor [23]. The modulated light is directed onto the PVDF pyroelectric sensor. The sample to be analyzed is placed on top of the sensor, using the thermal paste to ensure good thermal contact between the PVDF and the sample (as shown in Fig. 2).

Following that, the experimental data was fitted to the theoretical equation for the IPPE configuration, represented by Eq. (5), using the following expression [23]:

$$\theta(\omega) = \frac{(1-e^{\sigma_p l_p})(1+b) + (e^{-\sigma_p l_p} - 1)(1-b)}{(g-1)e^{-\sigma_p l_p}(1-b) + (g+1)e^{\sigma_p l_p}(1+b)}. \quad (5)$$

In Eq. (5), the variable $\theta(\omega)$ represents the average temperature in the pyroelectric detector, which is proportional to the PPE signal. The parameter l_p corresponds to the thickness of the pyroelectric sensor, (9 μm). Additionally, the parameter b is a fitting parameter used in the equation.

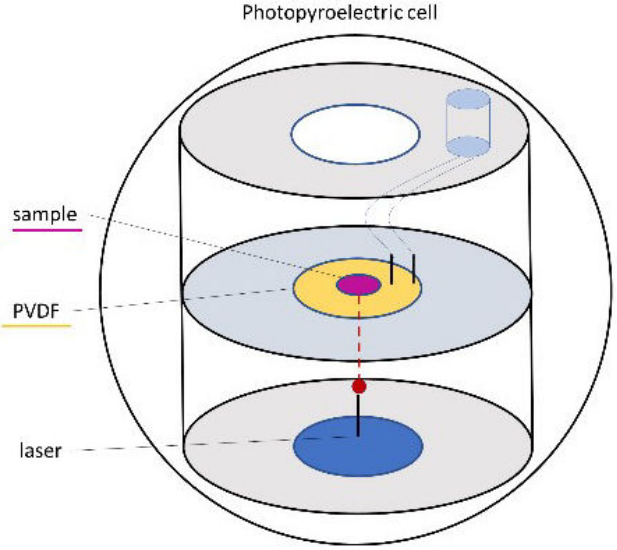

FIGURE 2. Experimental set up of IPPE.

$b = e_s/e_p$, e_s: thermal effusivity of the sample, e_p: thermal effusivity of the pyroelectric, $g = e_g/e_p$, e_g: thermal effusivity of gas (air) $\mu_s = 1/a_s$, μ: thermal diffusion length.

Finally, the thermal effusivity e of the sample can be determined using the following equation:

$$e_s = be_p. \quad (6)$$

Thermal conductivity and heat capacity per unit volume

To comprehensively characterize the studied sample, it is crucial to know its thermal conductivity (κ) and heat capacity per unit volume (ρc). These parameters can be directly determined by establishing the relationship between the thermal effusivity e_s, thermal conductivity (κ), thermal diffusivity (α), and volumetric heat capacity (ρc).

$$\kappa = e_s\sqrt{\alpha} \qquad \rho c = \frac{e_s}{\sqrt{\alpha}}. \quad (7)$$

Both samples were analyzed at a 0.120 mg/mL concentration, with bidistilled water as the suspension medium.

3. Results

Two types of nanoparticles were synthesized following the procedure outlined in Sec. 2. The first type is referred to as MNPs, which are magnetite nanoparticles obtained using the coprecipitation iron salt method and are used as a reference. The second type is MNPs@ $C_{96}H_{104}O_{20}$, which refers to magnetite nanoparticles directly coated with TE (turmeric extract).

Particle size and coating

TEM and DLS analysis was conducted to observe the nanometric size and semi-spherical morphology of the synthesized magnetite nanoparticles, as shown in Fig. 3. The particle size distribution was determined and presented in the

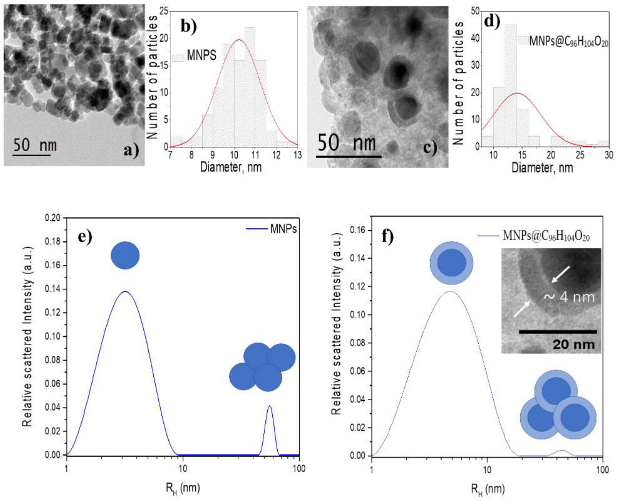

FIGURE 3. TEM micrographs for a), b) MNPs and c), d) MNPs@$C_{96}H_{104}O_{20}$samples. In (f inset) the organic cover over the nanoparticles is indicate by the white arrows. The histograms b), d) show the mean particle size fitted to Gaussian functions. DLS hydrodynamic radius are shown in e), f) for MNPs and MNPs@$C_{96}H_{104}O_{20}$ respectively. The second particle size populations could be associated with the particle aggregation of the samples.

TEM histogram. The mean particle size, represented as $\langle\phi\rangle$, was calculated from the Gaussian fitting. The average particle size of MNPs was determined to be $\phi = 10 \pm 1$ nm, as illustrated in Fig. 3b). In contrast, the average particle size for MNPs@$C_{96}H_{104}O_{20}$ (magnetite nanoparticles coated with Curcuma longa extract) was $\phi = 14 \pm 4$ nm, as indicated in Fig. 3d). By DLS, the MNPs sample showed two main particle size populations [Fig. 3e)]. The first one, with an average hydrodynamic radius of RH: 3 ± 1 nm and the second with RH: 55 nm. Similarly, the MNPs@$C_{96}H_{104}O_{20}$ sample [Fig. 3f)] shows one population with RH: 4 ± 2 nm, and the second one with RH: 44 nm. The second population represents the particle aggregates due to their magnetization. The organic shell thickness corresponding to the TE polyphenols in the MNPs@$C_{96}H_{104}O_{20}$ sample was observed by TEM and measured over low-contrast areas ($\sim$ 4 nm), as shown in the inset of Fig. 3f). The MNPs and MNPs@$C_{96}H_{104}O_{20}$ samples showed nanoparticles in polydispersion using both techniques, which could be due to their magnetic properties that favor particle aggregation of the samples.

Thermal diffusivity

Figure 4 shows the experimental PPE signal phase as a function of the Relative sample thickness; the blue circles represent the experimental values for the MNPs@$C_{96}H_{104}O_{20}$ and the black MNPs. According to Eq. (4), from the linear fit (red line) of the photopyroelectric signal phase (shown in Fig. 4), the sample thermal diffusivity α can be obtained (see Table I).

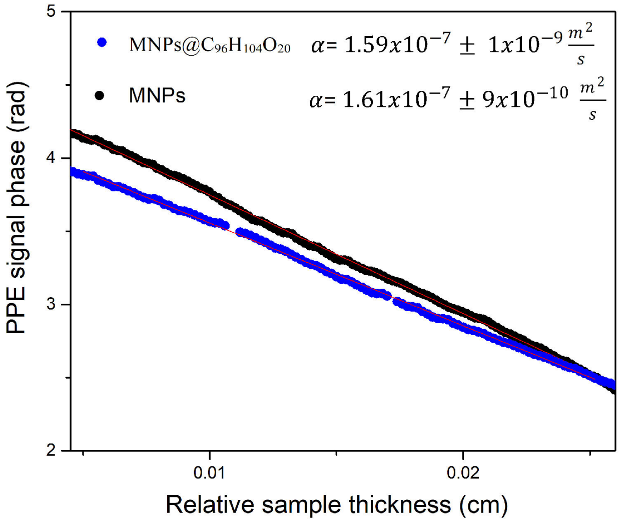

FIGURE 4. Thermal diffusivity obtained by fitting the experimental data of TWRC signals.

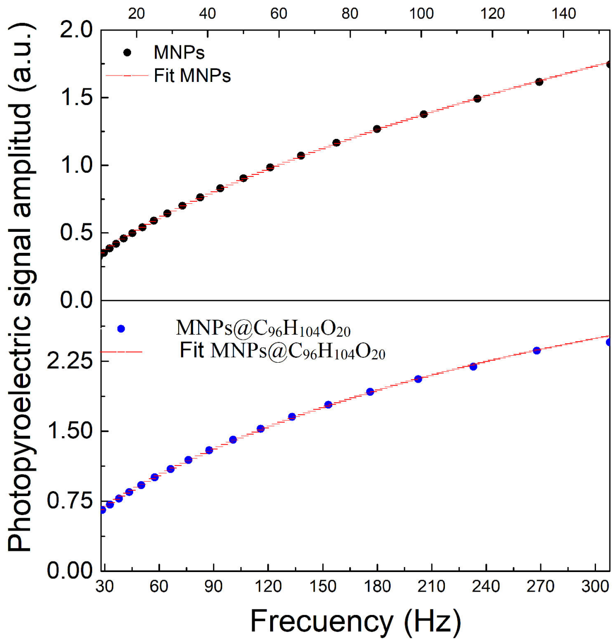

FIGURE 5. Fit of Eq. (5) (red continuous line) to the IPPE signal experimental data.

Thermal effusivity

From the fit of Eq. (5) to the experimental data obtained from the photopyroelectric signal as a function of frequency, the fit parameter b was obtained (Fig. 5), and the thermal effusivity of the samples e_s, knowing that the pyroelectric thermal effusivity is $e_p = 530\ \mathrm{W}\sqrt{s}/\mathrm{m}^2\mathrm{K}$, was obtained using Eq. (6) (see Table I).

Thermal conductivity and heat capacity per unit volume

Finally, the thermal conductivity κ, and heat capacity per unit volume ρc, were calculated using Eq. (7) and are listed in Table I.

TABLE I. Thermal parameters and dimensional values of MNPs and MNPs@$C_{96}H_{104}O_{20}$.

Sample	RH DLS (nm)	Radious TEM(nm)	e_s $(\frac{W\sqrt{s}}{m^2K})$	α $(\frac{m^2}{s})$	κ $(\frac{W}{mK})$	ρc $(\frac{J}{m^3K})$ 1×10^6
MNPs	3 ± 1	5 ± 0.5	1484.42±54.31	$1.61\times10^{-7}\pm9\times10^{-10}$	0.59 ± 0.02	3.70 ± 0.13
MNPs@$C_{96}H_{104}O_{20}$	4 ± 2	7 ± 2	1349.32 ± 43.27	$1.59\times10^{-7}\pm1\times10^{-9}$	0.53 ± 0.01	3.38 ± 0.10
WATER*	N/A	N/A	1581.17	1×10^{-7}	0.60	4.16

*Data obtained from [29], N/A: not applicable.

Previous studies on MNPs have shown that several factors influence the values of e_s, α, κ, and ρc. Raykar *et al.* synthesized MNPs suspensions in ethylene glycol with a particle size of approximately 200 nm and uniform distribution. The thermal effusivity, diffusivity, and conductivity values obtained were 930 W$\sqrt{\text{s}}$/m^{2}K, 1.04×10^{-7} m^{2}s and, 0.3 W/mk, respectively [24]. Horia *et al.* analyzed MNPs in powder form using a photoacoustic technique. They report that for nanoparticle sizes of 10.7 nm, 20.56 nm, and 30.43 nm the thermal parameters increased as the nanoparticle size increased [25]. Another study reported that for cubic nanostructures of MNPs, the thermal conductivity ratio of the nanofluids increased with an increase in temperature and volume fraction, reporting the highest enhancement of thermal conductivity at 40°C [26]. In addition, Hong *et al.* reported in their study that the thermal conductivity of a Fe nanofluid increases nonlinearly up to 18% as the volume fraction of particles increases up to 0.55 vol. % [27]. From the results in Table I, it is possible to appreciate that covering the nanoparticles with Turmeric extract reduces the value of the thermal parameters. For e_s, a percentage difference of 9 % was obtained, for α of 1.2 %, κ of 10 %, and ρc of 8.6 %, respectively; these differences reveal the effect of the shell on the MNPs falling their thermal properties, serving as a thermal insulator that generates resistance to the flow of heat. No previous works have been presented that analyze the effect of Turmeric extract shells on MNPs, so this study contributes to understanding its influence on thermal properties. The values obtained in this study and previous research by several authors mentioned above indicate that not only do the synthesis parameters affect the nanofluid properties [28], but multiple parameters, such as nanoparticle size, concentration, shape, temperature, and carrier liquid, also influence the nanoparticle thermal parameters and must be considered to obtain accurate values.

4. Conclusions

The thermal parameters of the analyzed samples were close to the thermal values reported of water. The carrier liquid contributes to thermal diffusivity and effusivity (on a smaller scale than diffusivity), impacting the thermal conductivity and heat capacity per unit volume parameters. The particle size distribution ($\sim$ 14 nm) in MNPs@$C_{96}H_{104}O_{20}$ showed a lower thermal response concerning the MNPs. Some polyphenols, including Turmeric, have been reported to provide thermal insulation [18, 30, 31]. These thermal differences indicate that the turmeric coating thickness directly influences their properties, acting as a thermal barrier layer on magnetite nanoparticles. These results can be considered in future versatile research such as biological areas or the additives and lubricant industry.

Acknowledgment

The authors acknowledge the partial financial support from CONAHCYT, SIP-IPN projects No. 20196252, 20220488, 20230447 and Marcos Moshinsky 2018 cathedra. M. L. Alvarado-Noguez thanks CONAHCYT for a postdoctoral fellowship from “Estancias Posdoctorales por México”. We also thank B.S. Jair, Bocanegra Flores, and Eng. Marcela Guerrero for technical support at the Physics Department, CINVESTAV-IPN.

---

1. H. Liang *et al.*, Porous yolk-shell Fe/Fe3O4 nanoparticles with controlled exposure of highly active Fe(0) for cancer therapy, *Biomaterials* **268** (2021) 120530, `https://doi.org/10.1016/j.biomaterials.2020.120530`.
2. Fe3O4 liposome for photothermal/chemo-synergistic inhibition of metastatic breast tumor, *Colloids and Surfaces A: Physicochemical and Engineering Aspects* **634** (2022) 127921, `https://doi.org/10.1016/j.colsurfa.2021.127921`.
3. R. P. Tardale, S. Suresh, and K. Ramesh, Performance and Emission Characteristics of SI Engine with Standard and Modified Piston with Turmeric Leaf Oil as Biofuel, *International Journal of Vehicle Structures and Systems* **13** (2021) 14, `https://doi.org/10.4273/ijvss.13.1.04`.
4. M. Yusefi *et al.*, Green synthesis of Fe3O4 nanoparticles for hyperthermia, magnetic resonance imaging and 5-fluorouracil car-

rier in potential colorectal cancer treatment, *Research on Chemical Intermediates* **47** (2021) 1789, `https://doi.org/10.1007/s11164-020-04388-1`.

5. K. Wang *et al.*, Fe_3O_4 Angelica sinensis polysaccharide nanoparticles as an ultralow-toxicity contrast agent for magnetic resonance imaging, *Rare Metals* **40** (2021) 2486, `https://doi.org/10.1007/s12598-020-01620-0`.
6. A. M. Beyene *et al.*, Curcumin Nanoformulations with Metal Oxide Nanomaterials for Biomedical Applications, Nanomaterials **11** (2021) 460, `https://doi.org/10.3390/nano11020460`.
7. Y. Guo *et al.*, Polyphenol-Containing Nanoparticles: Synthesis, Properties, and Therapeutic Delivery, *Advanced Materials* **33** (2021) 2007356, `https://doi.org/10.1002/adma.202007356`.
8. A. L. Ramirez-Nuñez *et al.*, In vitro magnetic hyperthermia using polyphenol-coated Fe_3O_4 Fe_2O_3 nanoparticles from Cinnamomun verum and Vanilla planifolia : the concert of green synthesis and therapeutic possibilities, *Nanotechnology* **29** (2018) 074001, `https://doi.org/10.1088/1361-6528/aaa2c1`.
9. M. L. Alvarado-Noguez *et al.*, Processing and Physicochemical Properties of Magnetite Nanoparticles Coated with Curcuma longa L. Extract, *Materials* **16** (2023) 3020, `https://doi.org/10.3390/ma16083020`.
10. S. A. H. Martínez *et al.*, Magnetic nanomaterials assisted nanobiocatalysis systems and their applications in biofuels production, *Fuel* **312** (2022) 122927, `https://doi.org/10.1016/j.fuel.2021.122927`.
11. J. A. John, M. S. Samuel, and E. Selvarajan, Immobilized cellulase on Fe3O4/GO/CS nanocomposite as a magnetically recyclable catalyst for biofuel application, *Fuel* **333** (2023) 126364, `https://doi.org/10.1016/j.fuel.2022.126364`.
12. R. Perveen *et al.*, Development of a ternerry condunting composite (PPy/Au/CNT@Fe3O4) immobilized FRT/GOD bioanode for glucose/oxygen biofuel cell applications, International *Journal of Hydrogen Energy* **46** (2021) 3259, `https://doi.org/10.1016/j.ijhydene.2020.02.175`.
13. A. Sundaramurthy, Phytosynthesized nanomaterials-NextGen material for biomedical applications (Elsevier, 2023), pp. 31, `https://doi.org/10.1016/B978-0-12-824373-2.00005-2`.
14. K. Mansouri *et al.*, Clinical effects of curcumin in enhancing cancer therapy: A systematic review, *BMC Cancer* **20** (2020), `https://doi.org/10.1186/s12885-020-07256-8`.
15. C. Huang *et al.*, Curcumin, demethoxycurcumin, and bisdemethoxycurcumin induced caspase-dependent and - independent apoptosis via Smad or Akt signaling pathways in HOS cells, *BMC complementary medicine and therapies* **20** (2020) 68, `https://doi.org/10.1186/s12906-020-2857-1`.
16. M. Mandal, P. Jaiswal, and A. Mishra, Role of curcumin and its nanoformulations in neurotherapeutics: A comprehensive review, *Journal of Biochemical and Molecular Toxicology* **34** (2020), `https://doi.org/10.1002/jbt.22478`.
17. A. Ruby *et al.*, Anti-tumour and antioxidant activity of natural curcuminoids, *Cancer Letters* **94** (1995) 79, `https://doi.org/10.1016/0304-3835(95)03827-J`.
18. X. Liu *et al.*, Utilization of turmeric residue for the preparation of ceramic foam, *Journal of Cleaner Production* **278** (2021) 123825, `https://doi.org/10.1016/j.jclepro.2020.123825`.
19. C. Gavimath and P. U. Raikar, Performance Characteristics of a Diesel Engine Fuelled with Biodiesel Produced from Mahua Oil Using Turmeric as a Fuel Additive, International Research Journal of Engineering and Technology (2015).
20. J. S. Rodrigues *et al.*, Comparative study of synthetic and natural antioxidants on the oxidative stability of biodiesel from Tilapia oil, *Renewable Energy* **156** (2020) 1100, `https://doi.org/10.1016/j.renene.2020.04.153`.
21. A. Alvis, G. Arrazola, and W. Martinez, Evaluación de la Actividad y el Potencial Antioxidante de Extractos Hidro-Alcohólicos de Cúrcuma (Cúrcuma longa), *Información tecnológica* **23** (2012) 11, `https://doi.org/10.4067/S0718-07642012000200003`.
22. P. M. P. D. P. Almond, Photothermal science and techniques, 1st ed. (Springer Dordrecht, 1996).
23. J. J. A. Flores-Cuautle, A. Cruz-Orea, and E. Suaste-Gómez, Thermal Effusivity of the Pb 0.88 Ln 0.08 Ti 0.98 Mn 0.02 O 3 (Ln=La, Eu) Ferroelectric Ceramic System by Inverse Photopyroelectric Technique, *Ferroelectrics* **386** (2009) 36, `https://doi.org/10.1080/00150190902961264`.
24. V. S. Raykar and A. K. Singh, Photoacoustic Method for Measurement of Thermal Effusivity of Fe 3 O 4 Nanofluid, *Journal of Thermodynamics* **2011** (2011) 1, `https://doi.org/10.1155/2011/464368`.
25. F. Horia *et al.*, Optical and Thermophysical Characterization of Fe 3 O 4 nanoparticle, *IOP Conference Series: Materials Science and Engineering* **956** (2020) 012016, `https://doi.org/10.1088/1757-899X/956/1/012016`.
26. M. Abareshi *et al.*, Fabrication, characterization and measurement of thermal conductivity of Fe_3O_4 nanofluids, *Journal of Magnetism and Magnetic Materials* **322** (2010) 3895, `https://doi.org/10.1016/j.jmmm.2010.08.016`.
27. T. K. Hong, H. S. Yang, and C. J. Choi, Study of the enhanced thermal conductivity of Fe nanofluids, *Journal of Applied Physics* **97** (2005), `https://doi.org/10.1063/1.1861145`.
28. N. S. Mane and V. Hemadri, Experimental Investigation of Stability, Properties and Thermo-rheological Behaviour of Water-Based Hybrid CuO and Fe3O4 Nanofluids, *International Journal of Thermophysics* **43** (2022) 7, `https://doi.org/10.1007/s10765-021-02938-2`.
29. A. Bejan and A. D. Kraus, Heat transfer handbook (J. Wiley, 2003), p. 1480.
30. Z. Xia *et al.*, Unraveling the mechanism of thermal and thermo-oxidative degradation of tannic acid, *Thermochimica Acta* **605** (2015) 77, `https://doi.org/10.1016/j.tca.2015.02.016`.
31. S. Basak *et al.*, Tannin based polyphenolic biomacromolecules: Creating a new era towards sustainable flame retardancy of polymers, *Polymer Degradation and Stability* **189** (2021), `https://doi.org/10.1016/j.polymdegradstab.2021.109603`.